Sliding mode voltage control of boost converters in DC microgrids

Cucuzzella, Michele; Lazzari, Riccardo; Trip, Sebastian; Rosti, Simone; Sandroni, Carlo; Ferrara, Antonella

Published in:
Control Engineering Practice

DOI:
10.1016/j.conengprac.2018.01.009

Publication date:
2018

Available online at www.sciencedirect.com

ScienceDirect

Control Engineering Practice 00 (2018) 1–12

Control Engineering Practice

Sliding mode voltage control of boost converters in DC microgrids*

Michele Cucuzzella[a,**], Riccardo Lazzari[b], Sebastian Trip[a], Simone Rosti[c], Carlo Sandroni[b], Antonella Ferrara[c]

[a] *Faculty of Science and Engineering, University of Groningen, Nijenborgh 4, 9747 AG Groningen, the Netherlands*
[b] *Department of Power Generation Technologies and Materials, RSE S.p.A., via Rubattino Raffaele 54, 20134 Milan, Italy*
[c] *Dipartimento di Ingegneria Industriale e dell'Informazione, University of Pavia, via Ferrata 5, 27100 Pavia, Italy*

Abstract

This paper deals with the design of a robust decentralized control scheme for voltage regulation in boost-based DC microgrids. The proposed solution consists of the design of a suitable manifold on which voltage regulation is achieved even in presence of unknown load demand and modelling uncertainties. A second order sliding mode control is used to constrain the state of the microgrid to this manifold by generating continuous control inputs that can be used as duty cycles of the power converters. The proposed control scheme has been theoretically analyzed and validated through experiments on a real DC microgrid.

Keywords: DC Microgrids, Sliding mode control, Decentralized control, Uncertain systems, Voltage regulation.

1. Introduction

Nowadays, due to economical, technological and environmental reasons, the most relevant challenge in power grids deals with the transition of the traditional power generation and transmission systems towards the large scale introduction of smaller Distributed Generation units (DGus) [1, 2, 3, 4]. Moreover, due to the ever-increasing energy demand and the public concern about global warming and climate change, much effort has been focused on the diffusion of environmentally friendly Renewable Energy Sources (RES) [5]. However, it is well known that when several DGus are interconnected to each other, issues such as voltage and frequency deviations arise together with protections problems [2, 6]. In this context, in order to integrate different types of RES and, in addition, electrify remote areas, the so-called *microgrids* have been proposed as a new concept of electric power systems [7, 8, 9]. Microgrids are electrical distribution networks, composed of clusters of DGus, loads, energy storage systems and energy conversion devices interconnected through power distribution lines and able to operate in islanded and grid-connected modes [10, 11, 12, 13].

Since electrical Alternating Current (AC) has been widely used in most industrial, commercial and residential applications, AC microgrids have attracted the attention of many control system researchers as well as power electronics and electrical engineers [14, 15, 16, 17, 18, 19, 20]. However, several advantages of DC microgrids with respect to AC microgrids are well known [21, 22]. The most important advantage relies on the natural interface of many types of RES, energy storage systems and loads (e.g. photovoltaic panels, batteries, electronic appliances and electric vehicles) with DC network, through DC-DC power converters. For this reason, lossy conversion stages are reduced and consequently DC microgrids are more efficient than AC microgrids. Furthermore, control systems for a DC microgrid are less complex than the ones required for an AC microgrid, where several issues such as synchronization, frequency regulation, reactive power flows, harmonics and unbalanced loads need to be addressed.

DC microgrids can operate in the so-called islanded operation mode to supply an isolated area or can be connected to existing AC networks (e.g. an AC microgrid or the main grid) through a DC-AC bidirectional converter, forming a so-called hybrid microgrid [23, 24], ensuring a high power quality level. Moreover, the growing need of interconnecting remote power

*This work has been financed by the Research Fund for the Italian Electrical System under the Contract Agreement between RSE S.p.A. and the Ministry of Economic Development - General Directorate for Nuclear Energy, Renewable Energy and Energy Efficiency in compliance with the Decree of March 8, 2006. This work is part of the EU Project 'ITEAM' [project number 675999]; and is part of the research programme ENBARK+ [project number 408.urs+.16.005], which is (partly) financed by the Netherlands Organisation for Scientific Research (NWO).

**This is the final version of the accepted paper submitted to Control Engineering Practice. Corresponding author

Email address: m.cucuzzella@rug.nl (Michele Cucuzzella)

networks (e.g. off-shore wind farms) has encouraged the use of High Voltage Direct Current (HVDC) technology, which is advantageous not only for long distances, but also for underwater cables, asynchronous networks and grids running at different frequencies [25]. Different control approaches have been investigated in the literature (see for instance [26, 27, 28] and the references therein). Finally, DC microgrids are widely deployed in avionics, data centres, traction power systems, manufacturing industries, and recently used in modern design for ships and large charging facilities for electric vehicles. For all these reasons, DC microgrids are attracting growing interest and receive much attention from the research community.

Two main control objectives in DC microgrids are voltage regulation and current or power sharing. Regulating the voltages is required to ensure a proper operation of connected loads, whereas current or power sharing prevents the overstressing of any source. Typically, both objectives are simultaneously achieved by designing hierarchical control schemes. In the literature, these control problems have been addressed by different approaches (see for instance [29, 30, 31, 32, 33, 34, 35, 36, 37, 38] and the references there in). All these works deal with DC-DC buck converters or do not take into account the model of the power converter. However, in many battery-powered applications such as hybrid electric vehicles and lighting systems, DC-DC boost converters can be used in order to achieve higher voltage and reduce the number of cells[1] [39, 40, 41]. Since the dynamics of the boost converter are nonlinear, regulating the output voltage in presence of unknown load demand and uncertain network parameters is not an easy task. For all these reasons, the solution in this paper relies on the Sliding Mode (SM) control methodology to solve the voltage control problem in boost-based DC microgrids affected by nonlinearities and uncertainties [42, 43, 44]. Indeed, sliding modes are well known for their robustness properties and, belonging to the class of Variable Structure Control Systems, have been extensively applied in power electronics, since they are perfectly adequate to control the inherently variable structure nature of DC-DC converters [45, 46, 47, 48, 49, 50]. SM controllers require to operate at very high (ideally infinite) and variable switching frequency. This condition increases the power losses and the issues related to the electromagnetic interference noise, making the design of the input and output filters more complicated [51]. SM controllers based on the hysteresis-modulation (also known as delta-modulation) have been proposed in order to restrict the switching frequency (see for instance [52]). To do this, additional tools such as constant timer circuits or adaptive hysteresis band are required, making the solution more elaborated and then unattractive. Moreover, this approach (called quasi-SM) reduces the robustness of the control system [53]. Alternatively, the so-called equivalent control approach and the application of state space averaging method to SM control have been proposed together with the Pulse Width Modulation (PWM) technique (otherwise known as duty cycle control) to achieve constant switching frequency [54]. However, computing the equivalent control often requires the perfect knowledge of the model parameters as well as the load and the input voltage [55], or the implementation of observers to estimate them [56]. Alternatively, in [57] a total SM controller has been proposed relying on the nominal model of a single boost converter and exploiting a discontinuous control law to reject the model uncertainties.

In this paper, in order to control the output voltage of boost converters in DC microgrids, a fully decentralized Second Order SM (SOSM) control solution is proposed, capable of dealing with unknown load and input voltage dynamics, as well as uncertain model parameters, without requiring the use of observers. Due to its decentralized and robust nature, the design of each low-level local controller does not depend on the knowledge of the whole microgrid, making the control synthesis simple, the control scheme scalable and suitable for be coupled with higher-level control schemes aimed at generating voltage references that guarantee load sharing. Since a higher order sliding modes methodology is used, the proposed controllers generate continuous inputs that can be used as duty cycles, in order to achieve constant switching frequency. Besides, being of higher order, a distinguishing feature of the proposed control scheme is that an additional auxiliary integral controller is coupled to the controlled converter, via suitable designed sliding function. Moreover, with respect to the existing literature (to the best of our knowledge) in this paper the local stability of a boost-based microgrid is analyzed, instead of the single boost converter, theoretically proving that on the obtained sliding manifold, the desired operating point is robustly locally exponentially stable. Additionally, the analysis is useful to choose suitable controller parameters ensuring the stability, and facilitates the tuning of the controllers. The proposed control scheme has been validated through experimental tests on a real DC microgrid test facility at Ricerca sul Sistema Energetico (RSE), in Milan, Italy [58], showing satisfactory closed-loop performances.

The present paper is organized as follows: Section 2 introduces the main concepts and the description of the considered system. In Section 3 the microgrid model is presented and the control problem is formulated, while in Section 4 the proposed SOSM is designed. In Section 5 the stability properties of the controlled system are theoretically analyzed, while in Section 6 the experimental results on a real DC microgrid are illustrated and discussed. Some conclusions are finally gathered in Section 7.

2. DC Microgrid Model

Before introducing the model of the considered boost-based DC microgrid, for the readers' convenience, some basic notions on DC microgrids are presented.

Fig. 1 shows the electrical scheme of a typical boost-based DC microgrid, where two DGus, with local loads, exchange power through the distribution line represented by the resistance R_{ij}. The energy source of a DGu, which can be of renewable type, is represented, for simplicity, by a DC voltage source V_{DC}. The boost converter feeds a local DC load with a voltage level V higher than V_{DC}. Note that, the boost converter allows to

[1] Battery-powered applications often stack cells in series to increase the voltage level.

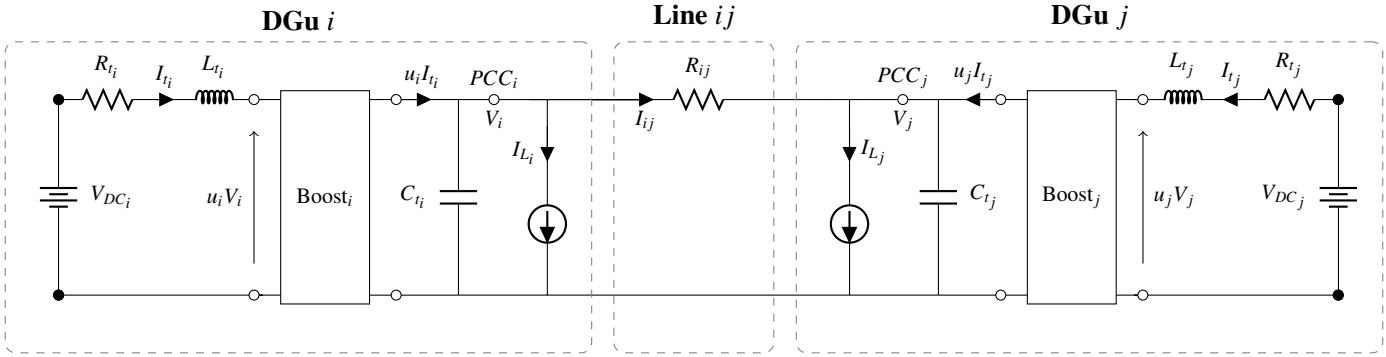

Figure 1. The considered electrical scheme of a typical boost-based DC microgrid composed of two DGus.

obtain an output voltage level higher than or equal to the voltage input. This is done due to the quick succession of two different operation stages during which the inductance L_t accumulates or supplies energy. The resistance R_t, instead, represents all the unavoidable energy losses. Finally the capacitor C_t is used in order to maintain a constant voltage at the output of the power converter. The local DC load is connected to the so-called Point of Common Coupling (PCC) and it can be treated as a current disturbance I_L.

The network is represented by a connected and undirected graph $\mathcal{G} = (\mathcal{V}, \mathcal{E})$, where the nodes $\mathcal{V} = \{1, ..., n\}$, represent the DGus and the edges $\mathcal{E} = \{1, ..., m\}$, represent the distribution lines interconnecting the DGus. First, consider the scheme reported in Fig. 1. By applying the Kirchhoff's current (KCL) and voltage (KVL) laws, and by using an average switching method, the governing dynamic equations[2] of the i-th node are the following

$$\begin{aligned} L_{t_i}\dot{I}_{t_i} &= -R_{t_i}I_{t_i} - u_i V_i + V_{DC_i} \\ C_{t_i}\dot{V}_i &= u_i I_{t_i} - I_{L_i} - \textstyle\sum_{j\in\mathcal{N}_i} I_{ij}, \end{aligned} \tag{1}$$

where $\mathcal{N}_i$ is the set of nodes (i.e., DGus) connected to the i-th DGu by distribution lines, while $u_i = 1 - d_i$ is the control input and d_i is the duty cycle ($0 \le d_i \le 1$). Exploiting the Quasi Stationary Line (QSL) approximation of power lines [59, 60], for each $j \in \mathcal{N}_i$, one has

$$I_{ij} = \frac{1}{R_{ij}}(V_i - V_j). \tag{2}$$

The symbols used in (1) and (2) are described in Table 1.

Remark 1. (Kron reduction) *Note that in* (1)*, the load currents are located only at the PCC of each DGu (see also Fig. 1). However, in many cases the loads are not close to the DGus. Then, by using the well known Kron reduction method, it is possible to map arbitrary interconnections of DGus (boundary nodes) and loads (interior nodes), into a reduced network with only local loads [31, 61].*

[2]For the sake of simplicity, the dependence of all the variables on time t is omitted throughout the paper.

Table 1. Description of the used symbols

	State variables
I_{t_i}	Inductor current
V_i	Boost output voltage
I_{ij}	Exchanged current
	Parameters
R_{t_i}	Filter resistance
L_{t_i}	Filter inductance
C_{t_i}	Shunt capacitor
R_{ij}	Line resistance
	Inputs
u_i	Control input
V_{DC_i}	Voltage source
I_{L_i}	Unknown current demand

The network topology can be represented by its corresponding incidence matrix $\mathbf{B} \in \mathbb{R}^{n\times m}$. The ends of edge k are arbitrarily labeled with a + and a −. More precisely, one has that

$$b_{ik} = \begin{cases} +1 & \text{if } i \text{ is the positive end of } k \\ -1 & \text{if } i \text{ is the negative end of } k \\ 0 & \text{otherwise.} \end{cases}$$

Let '$\circ$' denote the so-called Hadamard product (also known as Schur product). Given the vectors $\mathbf{p} \in \mathbb{R}^n, \mathbf{q} \in \mathbb{R}^n$, then $(\mathbf{p} \circ \mathbf{q}) \in \mathbb{R}^n$ with $(\mathbf{p} \circ \mathbf{q})_i = p_i q_i$ for all $i \in \mathcal{V}$. After substituting (2) in (1), the overall microgrid system can be written compactly for all nodes $i \in \mathcal{V}$ as

$$\begin{aligned} \mathbf{L_t}\dot{\boldsymbol{\imath}}_\mathbf{t} &= -\mathbf{R_t}\boldsymbol{\imath}_\mathbf{t} - \mathbf{u} \circ \mathbf{v} + \mathbf{v_{DC}} \\ \mathbf{C_t}\dot{\mathbf{v}} &= \mathbf{u} \circ \boldsymbol{\imath}_\mathbf{t} - \mathbf{B}\mathbf{R}^{-1}\mathbf{B}^T\mathbf{v} - \boldsymbol{\imath}_\mathbf{L}, \end{aligned} \tag{3}$$

where $\boldsymbol{\imath}_\mathbf{t} = [I_{t_1}, \dots, I_{t_n}]^T$, $\mathbf{v} = [V_1, \dots, V_n]^T$, $\mathbf{v_{DC}} = [V_{DC_1}, \dots, V_{DC_n}]^T$, $\boldsymbol{\imath}_\mathbf{L} = [I_{L_1}, \dots, I_{L_n}]^T$, and $\mathbf{u} = [u_1, \dots, u_n]^T$. Moreover $\mathbf{C_t}, \mathbf{L_t}$ and $\mathbf{R_t}$ are $n \times n$ positive definite diagonal matrices, while $\mathbf{R}$ is a $m \times m$ positive definite diagonal matrix, e.g. $\mathbf{R_t} = \text{diag}\{R_{t_1}, \dots, R_{t_n}\}$ and $\mathbf{R} = \text{diag}\{R_1, \dots, R_m\}$, with $R_k = R_{ij}$ for all $k \in \mathcal{E}$, where line k connects nodes i and j.

3. Problem Formulation

Before introducing the control problem and in order to permit the controller design in the next sections, the following assumption is introduced:

Assumption 1. (Available information) *The state variables I_{t_i} and V_i are locally available only at the i-th DGu. The network parameters $R_{t_i}, R_i, L_{t_i}, C_{t_i}$, the current disturbance I_{L_i}, and the voltage source V_{DC_i} are constant, unknown but bounded, with bounds a-priori known.*

Remark 2. (Decentralized control) *Since, according to Assumption 1, the values of I_{t_i} and V_i are available only at the i-th DGu, the control scheme to regulate the voltages needs to be fully decentralized.*

Remark 3. (Varying uncertainty) *Note that the parameter uncertainty, the current disturbance and the voltage source are required to be constant (Assumption 1) only to allow for a steady state solution and to theoretically analyze its stability. In fact, since a robust control strategy is adopted, Assumption 1 is not needed to reach and remain on the desired sliding manifold that is designed in Section 4.*

Note that given a constant current disturbance $\boldsymbol{\imath}_{\mathbf{L}}$, and a constant voltage source $\mathbf{v_{DC}}$, there exist a constant control input $\overline{\mathbf{u}}$ and a steady state solution $(\overline{\boldsymbol{\imath}}_{\mathbf{t}}, \overline{\mathbf{v}})$ to system (3) that satisfy

$$\begin{aligned} \overline{\boldsymbol{\imath}}_{\mathbf{t}} &= \mathbf{R_t}^{-1}\left(-\overline{\mathbf{u}} \circ \overline{\mathbf{v}} + \mathbf{v_{DC}}\right) \\ \mathbf{B}\mathbf{R}^{-1}\mathbf{B}^T\overline{\mathbf{v}} &= \overline{\mathbf{u}} \circ \overline{\boldsymbol{\imath}}_{\mathbf{t}} - \boldsymbol{\imath}_{\mathbf{L}}. \end{aligned} \tag{4}$$

The second line of (4) implies[3] that at the steady state the total generated current $\mathbf{1}_n^T(\overline{\mathbf{u}} \circ \overline{\boldsymbol{\imath}}_{\mathbf{t}})$ is equal to the total current demand $\mathbf{1}_n^T\boldsymbol{\imath}_{\mathbf{L}}$. To formulate the control objective, aiming at voltage regulation, it is assumed that for every DGu, there exists a desired reference voltage $V_i^\star$.

Assumption 2. (Desired voltage) *There exists a constant reference voltage $V_i^\star$ at the PCC, for all $i \in \mathcal{V}$.*

The objective is then formulated as follows: Given system (3), and given a $\mathbf{v}^\star = [V_1^\star, \dots, V_n^\star]^T$, we aim at designing a fully decentralized control scheme capable of guaranteeing voltage regulation, i.e.

Objective 1. (Voltage regulation)

$$\lim_{t\to\infty} \mathbf{v}(t) = \overline{\mathbf{v}} = \mathbf{v}^\star. \tag{5}$$

4. The Proposed Solution

In this section a fully decentralized Suboptimal Second Order Sliding Mode (SSOSM) low-level control scheme is proposed in order to achieve Objective 1, providing a continuous control input. As a first step, system (3) is augmented with additional state variables θ_i for all $i \in \mathcal{V}$, resulting in:

$$\begin{aligned} \mathbf{L_t}\dot{\boldsymbol{\imath}}_{\mathbf{t}} &= -\mathbf{R_t}\boldsymbol{\imath}_{\mathbf{t}} - \mathbf{u} \circ \mathbf{v} + \mathbf{v_{DC}} \\ \mathbf{C_t}\dot{\mathbf{v}} &= \mathbf{u} \circ \boldsymbol{\imath}_{\mathbf{t}} - \mathbf{B}\mathbf{R}^{-1}\mathbf{B}^T\mathbf{v} - \boldsymbol{\imath}_{\mathbf{L}} \\ \dot{\boldsymbol{\theta}} &= -\left(\mathbf{v} - \mathbf{v}^\star\right). \end{aligned} \tag{6}$$

The additional state $\boldsymbol{\theta}$ will be coupled to the control input $\mathbf{u}$ via the proposed control scheme, and its dynamics provide a form of integral action that is helpful to obtain the desired voltage regulation.

Now, to facilitate the discussion, some definitions are recalled that are essential to sliding mode control. To this end, consider system

$$\dot{\mathbf{x}} = \boldsymbol{\zeta}(\mathbf{x}, \mathbf{u}), \tag{7}$$

with $\mathbf{x} \in \mathbb{R}^n$, $\mathbf{u} \in \mathbb{R}^m$.

Definition 1. (Sliding function) *The sliding function $\boldsymbol{\sigma}(\mathbf{x}) : \mathbb{R}^n \to \mathbb{R}^m$ is a sufficiently smooth output function of system (7).*

Definition 2. (Sliding manifold) *The r–sliding manifold*[4] *is given by*

$$\left\{\mathbf{x} \in \mathbb{R}^n, \mathbf{u} \in \mathbb{R}^m : \boldsymbol{\sigma} = L_{\boldsymbol{\zeta}}\boldsymbol{\sigma} = \cdots = L_{\boldsymbol{\zeta}}^{(r-1)}\boldsymbol{\sigma} = \mathbf{0}\right\}, \tag{8}$$

where $L_{\boldsymbol{\zeta}}^{(r-1)}\boldsymbol{\sigma}(\mathbf{x})$ is the $(r-1)$-th order Lie derivative of $\boldsymbol{\sigma}(\mathbf{x})$ along the vector field $\boldsymbol{\zeta}(\mathbf{x}, \mathbf{u})$. With a slight abuse of notation, also $L_{\boldsymbol{\zeta}}\boldsymbol{\sigma}(\mathbf{x}) = \dot{\boldsymbol{\sigma}}(\mathbf{x})$, and $L_{\boldsymbol{\zeta}}^{(2)}\boldsymbol{\sigma}(\mathbf{x}) = \ddot{\boldsymbol{\sigma}}(\mathbf{x})$ are used in the remainder.

Definition 3. (Sliding mode order) *A r–order sliding mode is enforced from $t = T_r \geq 0$, when, starting from an initial condition, the state of (7) reaches the r–sliding manifold, and remains there for all $t \geq T_r$. The order of a sliding mode controller is identical to the order of the sliding mode that it is aimed at enforcing.*

Now, a suitable sliding function $\boldsymbol{\sigma}(\boldsymbol{\imath}_{\mathbf{t}}, \mathbf{v}, \boldsymbol{\theta})$ for system (6) will be introduced, that permits to prove the achievement of Objective 1. The choice is indeed motivated by the stability analysis in the next section, but it is stated here for the sake of exposition. First, the sliding function $\boldsymbol{\sigma} : \mathbb{R}^{3n} \to \mathbb{R}^n$ is given by

$$\boldsymbol{\sigma}(\boldsymbol{\imath}_{\mathbf{t}}, \mathbf{v}, \boldsymbol{\theta}) = \mathbf{M_1}\boldsymbol{\imath}_{\mathbf{t}} + \mathbf{M_2}(\mathbf{v} - \mathbf{v}^\star) - \mathbf{M_3}\boldsymbol{\theta}, \tag{9}$$

where $\mathbf{M_1} = \mathrm{diag}\{m_{1_1}, \dots, m_{1_n}\}$, $\mathbf{M_2} = \mathrm{diag}\{m_{2_1}, \dots, m_{2_n}\}$, $\mathbf{M_3} = \mathrm{diag}\{m_{3_1}, \dots, m_{3_n}\}$ are positive definite diagonal matrices suitable selected in order to assign the dynamics of system (3) when it is constrained on the manifold $\boldsymbol{\sigma} = \mathbf{0}$. Since $\mathbf{M_1}$, $\mathbf{M_2}$, $\mathbf{M_3}$ are diagonal matrices, $\sigma_i, i \in \mathcal{V}$, depends, according to Assumption 1, only on the state variables locally available at the i-th node, facilitating the design of a decentralized control scheme (see Remark 2).

[3] The incidence matrix $\mathbf{B}$ satisfies $\mathbf{1}_n^T\mathbf{B} = \mathbf{0}$, where $\mathbf{1}_n \in \mathbb{R}^n$ is the vector consisting of all ones.

[4] For the sake of simplicity, the order r of the sliding manifold is omitted in the remainder of this paper.

By regarding the sliding function (9) as the output function of system (3), it appears that the relative degree[5] of the system is one. This implies that a first order sliding mode controller can be *naturally* applied in order to attain in a finite time the sliding manifold $\boldsymbol{\sigma} = \mathbf{0}$ [42]. In this case, the discontinuous control signal generated by a first order sliding mode controller can be directly used to open and close the switch of the boost converter.

Remark 4. (Duty cycle) *By using a (discontinuous) first order sliding mode control law to open and close the switch of the boost converter, the Insulated Gate Bipolar Transistors (IGBTs) switching frequency cannot be a-priori fixed and the corresponding power losses could be very high. To overcome this issue, different techniques have been proposed in the literature (see for instance [62, 63, 64] and the references therein). In [62], fixed switching frequency is achieved by constraining the state of the controlled system in a neighbour of the sliding manifold (boundary layer approach), loosing the robustness property typical of SM control. In order to ensure a constant switching frequency, an adaptive hysteresis SM control and a load observer have been proposed in [63, 64], leading to more complicated controller implementations. However, in order to achieve a constant IGBTs switching frequency, boost converters are usually controlled by implementing the so-called Pulse Width Modulation (PWM) technique. To do this, a continuous control signal that represents the so-called duty cycle of the boost converter is required.*

Since sliding mode controllers generate a discontinuous control signal, in order to obtain a continuous control signal, the procedure suggested in [65] is adopted by integrating the discontinuous signal, yielding for system (6)

$$\begin{aligned} \mathbf{L_t}\dot{\boldsymbol{\imath}}_\mathbf{t} &= -\mathbf{R_t}\boldsymbol{\imath}_\mathbf{t} - \mathbf{u}\circ\mathbf{v} + \mathbf{v_{DC}} \\ \mathbf{C_t}\dot{\mathbf{v}} &= \mathbf{u}\circ\boldsymbol{\imath}_\mathbf{t} - \mathbf{B}\mathbf{R}^{-1}\mathbf{B}^T\mathbf{v} - \boldsymbol{\imath}_\mathbf{L} \\ \dot{\boldsymbol{\theta}} &= -(\mathbf{v} - \mathbf{v}^\star) \\ \dot{\mathbf{u}} &= \mathbf{h}, \end{aligned} \tag{10}$$

where $\mathbf{h} \in \mathbb{R}^n$ is the new (discontinuous) sliding mode control input. From (10) one can observe that the system relative degree (with respect to the new control input $\mathbf{h}$) is now two. Then, it is possible to rely on second order sliding mode control strategy in order to steer the state of system (10) to the sliding manifold $\boldsymbol{\sigma} = \dot{\boldsymbol{\sigma}} = \mathbf{0}$ for all $t \geq T_r$. To make the controller design explicit, a specific second order sliding mode controller is discussed, namely, the well known 'Suboptimal Second Order Sliding Mode' (SSOSM) controller proposed in [65].

Define d_i equal to $\sum_{j\in\mathcal{N}_i} I_{ij}$, with I_{ij} given by (2). For each node two auxiliary variables are defined, $\xi_{1_i} = \sigma_i$ and $\xi_{2_i} = \dot{\sigma}_i, i \in \mathcal{V}$, and the so-called auxiliary system is build as follows:

$$\begin{aligned} \dot{\xi}_{1_i} &= \xi_{2_i} \\ \dot{\xi}_{2_i} &= \phi_i(\dot{I}_{t_i}, \dot{V}_i, \dot{d}_i, u_i) - \gamma_i(I_{t_i}, V_i)h_i \\ \dot{u}_i &= h_i, \end{aligned} \tag{11}$$

where ξ_{2_i} is not measurable. Indeed, according to Assumption 1, I_{L_i} is unknown and the parameters of the model are uncertain. Bearing in mind that $\dot{\xi}_{2_i} = \ddot{\sigma}_i = \phi_i + \gamma_i h_i$, the expressions for ϕ_i and γ_i are straightforwardly obtained from (9) by taking the second derivative of σ_i with respect to time, yielding

$$\begin{aligned} \phi_i(\cdot) &= -m_{1_i}L_{t_i}^{-1}R_{t_i}\dot{I}_{t_i} + m_{3_i}\dot{V}_i - m_{1_i}L_{t_i}^{-1}\dot{V}_i u_i \\ &\quad + m_{2_i}C_{t_i}^{-1}\dot{I}_{t_i}u_i - m_{2_i}C_{t_i}^{-1}\dot{d}_i \\ \gamma_i(\cdot) &= m_{1_i}L_{t_i}^{-1}V_i - m_{2_i}C_{t_i}^{-1}I_{t_i}. \end{aligned} \tag{12}$$

The following assumption is made on the uncertainties ϕ_i and $\gamma_i, i \in \mathcal{V}$.

Assumption 3. (Bounded uncertainty) *Functions ϕ_i and γ_i in* (11) *have known bounds, i.e.,*

$$|\phi_i(\cdot)| \leq \Phi_i \qquad \forall i \in \mathcal{V}, \tag{13}$$

$$0 < \Gamma_{\min_i} \leq \gamma_i(\cdot) \leq \Gamma_{\max_i} \qquad \forall i \in \mathcal{V}, \tag{14}$$

Φ_i, $\Gamma_{\min_i}$ and $\Gamma_{\max_i}$ being positive constants.

Remark 5. (Adaptive SSOSM) *Note that in practical cases the bounds in* (13) *and* (14) *can be determined relying on data analysis and physical insights. However, if these bounds cannot be a-priori estimated, the adaptive version of the SSOSM algorithm proposed in [66] can be used to dominate the effect of the uncertainties.*

With reference to [65], for each DGu $i \in \mathcal{V}$, the control law that is proposed to steer ξ_{1_i} and ξ_{2_i}, to zero in a finite time can be expressed as

$$h_i = \alpha_i H_{\max_i} \operatorname{sgn}\left(\xi_{1_i} - \frac{1}{2}\xi_{1,\max_i}\right), \tag{15}$$

with

$$H_{\max_i} > \max\left(\frac{\Phi_i}{\alpha_i^*\Gamma_{\min_i}}; \frac{4\Phi_i}{3\Gamma_{\min_i} - \alpha_i^*\Gamma_{\max_i}}\right), \tag{16}$$

$$\alpha_i^* \in (0,1] \cap \left(0, \frac{3\Gamma_{\min_i}}{\Gamma_{\max_i}}\right), \tag{17}$$

α_i switching between α_i^* and 1, according to [65, Algorithm 1]. Note that the control input $u_i(t) = \int_0^t h_i(\tau)d\tau$, is continuous, since w_i is piecewise constant. Then, $d_i = 1 - u_i$ can be used as duty cycle of the i-th boost converter. The extremal values $\xi_{1,\max_i}$ in (15) can be detected by implementing for instance a peak detector as in [67]. Note also that the design of the local controller for each DGu is not based on the knowledge of the whole microgrid, making the control synthesis simpler and the proposed control scheme scalable.

Remark 6. (Alternative SOSM controllers) *In this work the control scheme relies on the SSOSM control law proposed in [65]. However, to constrain system* (10) *on the sliding manifold $\boldsymbol{\sigma} = \dot{\boldsymbol{\sigma}} = \mathbf{0}$, any other SOSM control law that does not need the measurement of $\dot{\boldsymbol{\sigma}}$ can be used (e.g. the super-twisting control algorithm [68]).*

[5] The relative degree is the minimum order ρ of the time derivative $\sigma_i^{(\rho)}, i \in \mathcal{V}$, of the sliding function associated to the i-th node in which the control $u_i, i \in \mathcal{V}$, explicitly appears.

5. Stability Analysis And Tuning Guidelines

In this section the (local) stability of the desired steady state $(\bar{\imath}_{\mathbf{t}}, \mathbf{v}^\star, \overline{\boldsymbol{\theta}})$ is studied, satisfying under an appropriate control input $\overline{\mathbf{u}}$ the steady state equations

$$\begin{aligned} \mathbf{0} &= -\mathbf{R_t}\bar{\imath}_{\mathbf{t}} - \overline{\mathbf{u}} \circ \mathbf{v}^\star + \mathbf{v_{DC}} \\ \mathbf{0} &= \overline{\mathbf{u}} \circ \bar{\imath}_{\mathbf{t}} - \mathbf{B}\mathbf{R}^{-1}\mathbf{B}^T\mathbf{v}^\star - \imath_{\mathbf{L}} \\ \mathbf{0} &= -(\mathbf{v}^\star - \mathbf{v}^\star). \end{aligned} \tag{18}$$

As will be shown, the stability analysis provides guidelines on the proper selection of the parameters appearing in the designed sliding function (9). First, one notices that the proposed SSOSM control scheme ensures that, after a finite time, the system (6) is constrained to the manifold characterized by $\boldsymbol{\sigma} = \dot{\boldsymbol{\sigma}} = \mathbf{0}$. This is made explicit in the following lemma:

Lemma 1. (Convergence to the sliding manifold) *Let Assumptions 1-3 hold. The solutions to system (6), controlled via the SSOSM control law (11)–(17), converge in a finite time T_r, to the sliding manifold $\{(\imath_{\mathbf{t}}, \mathbf{v}, \boldsymbol{\theta}) : \boldsymbol{\sigma} = \dot{\boldsymbol{\sigma}} = \mathbf{0}\}$, with $\boldsymbol{\sigma}$ given by (9).*

Proof. Following [65], the application of (11)–(17) to each converter guarantees that $\boldsymbol{\sigma} = \dot{\boldsymbol{\sigma}} = \mathbf{0}$, for all $t \geq T_r$. The details are omitted, since they are an immediate consequence of the used SSOSM control algorithm [65]. ∎

To continue the stability analysis, the so-called equivalent control is introduced, that permits to characterize the input $\mathbf{u}$ to the system once the sliding manifold is attained.

Definition 4. (Equivalent control) *Consider system* (7) *and the sliding function $\boldsymbol{\sigma}$. Assume that a r–order sliding mode exists on the manifold* (8)*. Assume also that a solution to system $\boldsymbol{\sigma}^{(r)} = L_\zeta^{(r)}\boldsymbol{\sigma} = \mathbf{0}$, with respect to the control input $\mathbf{u}$, exists. This solution is called equivalent control and is denoted by $\mathbf{u_{eq}}$ [42].*

Particularly, the dynamics of (7) are described on the sliding manifold by the so-called equivalent system that is obtained by substituting $\mathbf{u_{eq}}$ for $\mathbf{u}$. For the system at hand, the corresponding equivalent control is given by

$$\begin{aligned} \mathbf{u_{eq}} = &\left(\mathbf{M_1}\mathbf{L_t}^{-1}\mathrm{diag}(\mathbf{v}) - \mathbf{M_2}\mathbf{C_t}^{-1}\mathrm{diag}(\imath_{\mathbf{t}})\right)^{-1} \\ &\cdot (-\mathbf{M_1}\mathbf{L_t}^{-1}\mathbf{R_t}\imath_{\mathbf{t}} - \mathbf{M_2}\mathbf{C_t}^{-1}\mathbf{B}\mathbf{R}^{-1}\mathbf{B}^T\mathbf{v} \\ &+ \mathbf{M_1}\mathbf{L_t}^{-1}\mathbf{v_{DC}} - \mathbf{M_2}\mathbf{C_t}^{-1}\imath_{\mathbf{L}} + \mathbf{M_3}(\mathbf{v} - \mathbf{v}^\star)). \end{aligned} \tag{19}$$

The (global) stability study of the resulting nonlinear equivalent system is postponed to a future research. Instead, the focus here is on a local stability result, providing guidelines to the design of the control parameters. Therefore, system (6) is linearized around the point $(\bar{\imath}_{\mathbf{t}}, \mathbf{v}^\star, \overline{\boldsymbol{\theta}})$, resulting in the linearized system

$$\begin{aligned} \mathbf{L_t}\dot{\imath}_{\mathbf{t}} &= -\mathbf{R_t}(\imath_{\mathbf{t}} - \bar{\imath}_{\mathbf{t}}) - \overline{\mathbf{u}} \circ (\mathbf{v} - \mathbf{v}^\star) - \mathbf{v}^\star \circ (\mathbf{u} - \overline{\mathbf{u}}) \\ \mathbf{C_t}\dot{\mathbf{v}} &= \overline{\mathbf{u}} \circ (\imath_{\mathbf{t}} - \bar{\imath}_{\mathbf{t}}) + \bar{\imath}_{\mathbf{t}} \circ (\mathbf{u} - \overline{\mathbf{u}}) - \mathbf{B}\mathbf{R}^{-1}\mathbf{B}^T(\mathbf{v} - \mathbf{v}^\star) \\ \dot{\boldsymbol{\theta}} &= -(\mathbf{v} - \mathbf{v}^\star). \end{aligned} \tag{20}$$

Next, it is investigated how the linearized system behaves on the sliding manifold under the proposed sliding mode control scheme. The obtained equivalent system for (20) is determined explicitly in the following lemma:

Lemma 2. (Equivalent system) *For all $t \geq T_r$, the linearized dynamics of the controlled microgrid are given by the equivalent version of system (20) and are as follows:*

$$\begin{bmatrix} \dot{\tilde{\mathbf{v}}} \\ \dot{\tilde{\boldsymbol{\theta}}} \end{bmatrix} = \underbrace{\begin{bmatrix} \mathbf{F} & \mathbf{G} \\ -\mathbf{I} & \mathbf{0} \end{bmatrix}}_{\mathbf{A}} \begin{bmatrix} \tilde{\mathbf{v}} \\ \tilde{\boldsymbol{\theta}} \end{bmatrix}, \tag{21}$$

where $\tilde{\mathbf{v}} = \mathbf{v} - \mathbf{v}^\star$, $\tilde{\boldsymbol{\theta}} = \boldsymbol{\theta} - \overline{\boldsymbol{\theta}}$, and $\mathbf{I}$ is the identity matrix. Furthermore, the matrices $\mathbf{F}$ and $\mathbf{G}$ are given by

$$\begin{aligned} \mathbf{F} = &-\mathbf{M_1}^{-1}\mathbf{M_2}\mathrm{diag}(\overline{\mathbf{u}}) - \mathbf{B}\mathbf{R}^{-1}\mathbf{B}^T \\ &+ \mathbf{W}\mathbf{M_1}\mathbf{L_t}^{-1}\mathrm{diag}(\bar{\imath}_{\mathbf{t}})\left(\mathbf{M_1}^{-1}\mathbf{M_2}\mathbf{R_t} - \mathrm{diag}(\overline{\mathbf{u}})\right) \\ &- \mathbf{W}\mathbf{M_2}\mathbf{C_t}^{-1}\mathrm{diag}(\bar{\imath}_{\mathbf{t}})\left(\mathrm{diag}(\overline{\mathbf{u}})\mathbf{M_1}^{-1}\mathbf{M_2} + \mathbf{B}\mathbf{R}^{-1}\mathbf{B}^T\right) \\ &+ \mathbf{W}\mathbf{M_3}\mathrm{diag}(\bar{\imath}_{\mathbf{t}}), \end{aligned} \tag{22}$$

and

$$\begin{aligned} \mathbf{G} = &\mathbf{M_3}\mathbf{M_1}^{-1}\mathrm{diag}(\overline{\mathbf{u}}) - \mathbf{M_3}\mathbf{W}\mathbf{L_t}^{-1}\mathbf{R_t}\mathrm{diag}(\bar{\imath}_{\mathbf{t}}) \\ &+ \mathbf{M_3}\mathbf{W}\mathbf{M_2}\mathbf{M_1}^{-1}\mathbf{C_t}^{-1}\mathrm{diag}(\bar{\imath}_{\mathbf{t}})\mathrm{diag}(\overline{\mathbf{u}}), \end{aligned} \tag{23}$$

where

$$\mathbf{W} = \left(\mathbf{L_t}^{-1}\mathbf{M_1}\mathrm{diag}(\mathbf{v}^\star) - \mathbf{C_t}^{-1}\mathbf{M_2}\mathrm{diag}(\bar{\imath}_{\mathbf{t}})\right)^{-1}. \tag{24}$$

Proof. The relation $\dot{\boldsymbol{\sigma}} = \mathbf{0}$ is equivalent to

$$\mathbf{M_1}\dot{\imath}_{\mathbf{t}} + \mathbf{M_2}\dot{\mathbf{v}} - \mathbf{M_3}\dot{\boldsymbol{\theta}} = \mathbf{0}. \tag{25}$$

Bearing in mind the dynamics (20), equation (25) can be solved for $\mathbf{u}$, where it is additionally exploited that on the manifold $\boldsymbol{\sigma} = \mathbf{0}$ one has $\mathbf{M_1}\imath_{\mathbf{t}} = \mathbf{M_3}\boldsymbol{\theta} - \mathbf{M_2}(\mathbf{v} - \mathbf{v}^\star)$ and that at the point $(\bar{\imath}_{\mathbf{t}}, \mathbf{v}^\star, \overline{\boldsymbol{\theta}})$ it holds that $\mathbf{M_1}\bar{\imath}_{\mathbf{t}} = \mathbf{M_3}\overline{\boldsymbol{\theta}}$. This yields the following equivalent control $\mathbf{u_{eq}}$:

$$\begin{aligned} \mathbf{u_{eq}} = \overline{\mathbf{u}} + \mathbf{W}\Big(&\mathbf{M_1}\mathbf{L_t}^{-1}(-\mathbf{R_t}\tilde{\imath}_{\mathbf{t}} - \overline{\mathbf{u}} \circ \tilde{\mathbf{v}}) \\ &+ \mathbf{M_2}\mathbf{C_t}^{-1}(\overline{\mathbf{u}} \circ \tilde{\imath}_{\mathbf{t}} - \mathbf{B}\mathbf{R}^{-1}\mathbf{B}^T\tilde{\mathbf{v}}) + \mathbf{M_3}\tilde{\mathbf{v}}\Big), \end{aligned} \tag{26}$$

where $\tilde{\imath}_{\mathbf{t}} = \imath_{\mathbf{t}} - \bar{\imath}_{\mathbf{t}}$ and $\mathbf{W}$ is given by (24). Substituting $\mathbf{u_{eq}}$ for $\mathbf{u}$ in (20), and using again the relations $\mathbf{M_1}\imath_{\mathbf{t}} = \mathbf{M_3}\boldsymbol{\theta} - \mathbf{M_2}(\mathbf{v} - \mathbf{v}^\star)$ and $\mathbf{M_1}\bar{\imath}_{\mathbf{t}} = \mathbf{M_3}\overline{\boldsymbol{\theta}}$, it can be readily confirmed that the last two equations of (20) reduce to (21). ∎

As a consequence of the previous lemma, in order to prove that system (20) is exponentially stable on the attained sliding manifold, matrix $\mathbf{A}$ in (21) needs to be Hurwitz. However, explicitly characterizing all the eigenvalues of $\mathbf{A}$ is difficult, mainly due to the coupling term $\mathbf{B}\mathbf{R}^{-1}\mathbf{B}^T$. Generally, the eigenvalues depend indeed on the particular microgrid, its parameters and its operation point. However, in the remainder of this section, it is shown that, by LaSalle's invariance principle, the desired operating point of the controlled microgrid can always be made locally exponentially stable by choosing appropriate values for $\mathbf{M_1}, \mathbf{M_2}$ and $\mathbf{M_3}$ in the controller. Bearing in mind that system (21) is linear, the (local) exponential stability of (21) is indeed identical to matrix $\mathbf{A}$ being Hurwitz. Before continuing the stability analysis of (21), it is noted that in any practical case, the filter resistance is negligible, i.e. $\mathbf{R_t} \approx \mathbf{0}$. This leads to the following result on $\mathbf{G}$ given by (23).

Lemma 3. (Positive definiteness of (23)**)** *Let Assumption 3 hold. The matrix* $\mathbf{G}$ *in* (23) *is positive definite.*

Proof. The matrix $\mathbf{M_3}$ in (9) is positive definite, and as a consequence of Assumption 3 also the matrix $\mathbf{W} = \text{diag}\{w_1, \dots, w_n\}$ is positive definite, since w_i is the steady state value of $\gamma_i(\cdot) > 0$. From (23), we have

$$(\mathbf{M_3 W L_t}^{-1})^{-1}\mathbf{G} = \text{diag}(\overline{\mathbf{u}})\text{diag}(\mathbf{v}^\star) - \mathbf{R_t}\text{diag}(\bar{\boldsymbol{\iota}}_\mathbf{t}). \tag{27}$$

Since $\mathbf{R_t} \approx \mathbf{0}$ and the entries of $\overline{\mathbf{u}}$ and $\mathbf{v}^\star$ are positive, it follows that $\mathbf{G} > \mathbf{0}$. ∎

Exploiting Lemma 3 above, it is possible to suggest a suitable Lyapunov function to study the stability of system (21), or equally, the stability of (20) on the sliding manifold.

Proposition 1. (Sufficient condition for local exponential stability). *Let Assumptions 1-3 hold. The desired operating point* $(\bar{\boldsymbol{\iota}}_\mathbf{t}, \mathbf{v}^\star, \overline{\boldsymbol{\theta}})$*, satisfying* (18) *can be made locally exponentially stable on the sliding manifold characterized by* $\boldsymbol{\sigma} = \dot{\boldsymbol{\sigma}} = \mathbf{0}$*, by choosing the entries of* $\mathbf{M_2}$ *sufficiently large.*

Proof. Consider the Lyapunov function

$$S(\tilde{\mathbf{v}}, \tilde{\boldsymbol{\theta}}) = \tilde{\mathbf{v}}^T\tilde{\mathbf{v}} + \tilde{\boldsymbol{\theta}}^T\mathbf{G}\tilde{\boldsymbol{\theta}}, \tag{28}$$

where $\mathbf{G} > \mathbf{0}$ follows from Lemma 3. A straightforward calculation shows that $S(\tilde{\mathbf{v}}, \tilde{\boldsymbol{\theta}})$ satisfies along the solutions to (21)

$$\dot{S}(\tilde{\mathbf{v}}, \tilde{\boldsymbol{\theta}}) = \tilde{\mathbf{v}}^T(\mathbf{F} + \mathbf{F}^T)\tilde{\mathbf{v}} \leq 0. \tag{29}$$

From (22) we have

$$\begin{aligned}\mathbf{W}^{-1}\mathbf{F} = &- \mathbf{M_2 L_t}^{-1}\left(\text{diag}(\overline{\mathbf{u}})\text{diag}(\mathbf{v}^\star) - \mathbf{R_t}\text{diag}(\bar{\boldsymbol{\iota}}_\mathbf{t})\right)\\ &- \mathbf{M_1 L_t}^{-1}\text{diag}(\overline{\mathbf{u}})\text{diag}(\bar{\boldsymbol{\iota}}_\mathbf{t}) + \mathbf{M_3}\text{diag}(\bar{\boldsymbol{\iota}}_\mathbf{t})\\ &- \mathbf{M_1 B R}^{-1}\mathbf{B}^T\mathbf{L_t}^{-1}\text{diag}(\mathbf{v}^\star).\end{aligned} \tag{30}$$

Since $\mathbf{R_t} \approx \mathbf{0}$, then by choosing the entries of $\mathbf{M_2}$ sufficiently large, the diagonal of $\mathbf{F}$ can be made sufficiently negative such that $\mathbf{F} + \mathbf{F}^T < \mathbf{0}$. By LaSalle's invariance principle, the solutions to (21) converge to the largest invariant set where $\tilde{\mathbf{v}} = \mathbf{0}$. Moreover, on this invariant set it holds, due to the invertibility of $\mathbf{G}$, that $\tilde{\boldsymbol{\theta}} = \mathbf{0}$. Therefore, the solutions to (21) converge to the origin. This in turn implies that all the eigenvalues of $\mathbf{A}$ are negative, and consequently (21) is exponentially stable. Furthermore, since on the sliding manifold one has that $\boldsymbol{\sigma} = \mathbf{0}$, the local exponential stability of $\tilde{\mathbf{v}}$ and $\tilde{\boldsymbol{\theta}}$, implies that $\boldsymbol{\iota}_\mathbf{t}$ converges exponentially to $\mathbf{M_1}^{-1}\mathbf{M_3}\overline{\boldsymbol{\theta}}$. ∎

Remark 7. (Tuning rules) *First, we notice that for any* $i \in \mathcal{V}$*, the requirement of* $\gamma_i(\cdot) > 0$ *in Assumption 3 provides the following tuning rule*

$$m_{1_i} > \frac{L_{t_i}\bar{I}_{t_i}}{C_{t_i}V_i^\star}m_{2_i} \qquad \text{if } \bar{I}_{t_i} > 0. \tag{31}$$

If instead $\bar{I}_{t_i} \leq 0$*, then* $\gamma_i(\cdot)$ *is positive for any* m_{1_i}, m_{2_i}*. Secondly, one can notice that under the assumption of constant current exchanged with the neighbouring nodes,* $\mathbf{F}$ *becomes a diagonal matrix. Then, a tedious, but straightforward, calculation provides explicit bounds on the permitted values of* $\mathbf{M_1}, \mathbf{M_2}$ *and* $\mathbf{M_3}$ *such that the dynamics matrix*

$$\mathbf{A}_i = \begin{bmatrix} F_i & G_i \\ -1 & 0 \end{bmatrix} \in \mathbb{R}^{2\times 2} \tag{32}$$

of the i-th boost converter is Hurwitz for any $i \in \mathcal{V}$*, i.e.,*

$$\begin{aligned} m_{1_i} &> \frac{L_{t_i}}{\overline{u}_i}m_{3_i} + \frac{R_{t_i}}{\overline{u}_i}m_{2_i} - \frac{V_i^\star}{\bar{I}_{t_i}}m_{2_i} \qquad \text{if } \bar{I}_{t_i} > 0\\ m_{1_i} &< \frac{L_{t_i}}{\overline{u}_i}m_{3_i} + \frac{R_{t_i}}{\overline{u}_i}m_{2_i} - \frac{V_i^\star}{\bar{I}_{t_i}}m_{2_i} \qquad \text{if } \bar{I}_{t_i} \leq 0. \end{aligned} \tag{33}$$

Finally, combining (31) *and* (33)*, we have that*

$$\underline{\mu}_i < m_{1_i} < \overline{\mu}_i, \tag{34}$$

with

$$\begin{aligned} \underline{\mu}_i &= \max\left(\frac{L_{t_i}}{\overline{u}_i}m_{3_i} + \frac{R_{t_i}}{\overline{u}_i}m_{2_i} - \frac{V_i^\star}{|\bar{I}_{t_i}|}m_{2_i}; \frac{L_{t_i}|\bar{I}_{t_i}|}{C_{t_i}V_i^\star}m_{2_i}\right)\\ \overline{\mu}_i &= \frac{L_{t_i}}{\overline{u}_i}m_{3_i} + \frac{R_{t_i}}{\overline{u}_i}m_{2_i} + \frac{V_i^\star}{|\bar{I}_{t_i}|}m_{2_i}. \end{aligned} \tag{35}$$

6. Experimental Results

In order to verify the proposed control strategy, experimental tests have been carried out using the DC microgrid test facility at RSE, shown in Figs. 2–4. The controller parameters suggested by the stability results in the previous section were very useful for conducting the experiments. The RSE's DC grid is unipolar with a nominal voltage of 380 V and, during the test, includes one resistive load, with a maximum power of 30 kW at 400 V, one DC generator with a maximum power of 30 kW, that can be used as a PV emulator, and two Energy Storage Systems, based on high temperature NaNiCl batteries, each of them with an energy of 18 kWh and a maximum power of 30 kW for 10 s. These components are connected to a common DC link through four 35 kW DC-DC boost synchronous converters. The DC-DC converters are distributed and connected to the DC link with power distribution lines characterized by different parameters, as reported in Table 2.

The control of each converter is realized through two dSpace controllers that measure the inductor current and the boost output voltage and drive the power electronic converters. The DC-DC converters of the load and of the generator have input voltages equal to 266 V and 320 V, respectively. They are controlled in constant power mode and are treated, during the test, as current disturbances (see Fig. 2). The bidirectional converters of the batteries are controlled through the SSOSM control strategy described in Section 4, in order to regulate the voltage at Node 2 and Node 4 (see Fig. 2). The voltage reference $V^\star$

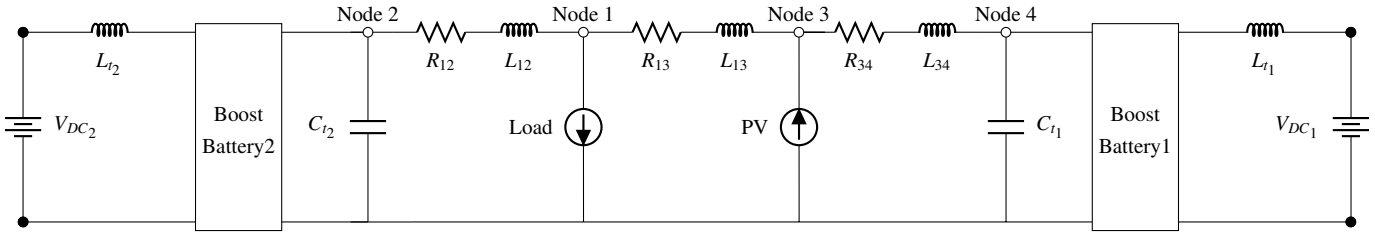

Figure 2. The considered electrical scheme of the RSE's DC microgrid adopted during the test.

Figure 3. Photo of the RSE's DC microgrid adopted during the test.

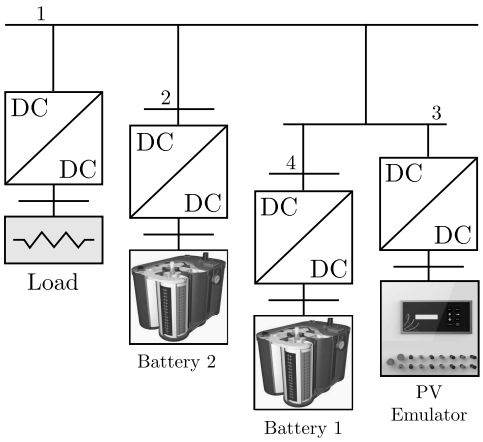

Figure 4. Layout of the RSE's DC microgrid adopted during the test.

Table 2. RSE DC Microgrid parameters

Symbol	Value	Unit	Description
V_{DC_1}, V_{DC_2}	278	V	Batteries nominal voltage
$V^\star$	380	V	DC network nominal voltage
R_{12}	250	mΩ	Tie-Line resistance 1-2
R_{13}	39	mΩ	Tie-Line resistance 1-3
R_{34}	250	mΩ	Tie-Line resistance 3-4
L_{12}	140	μH	Tie-Line inductance 1-2
L_{13}	86	μH	Tie-Line inductance 1-3
L_{34}	140	μH	Tie-Line inductance 3-4
C_{t_1}, C_{t_2}	6.8	mF	Output capacitances
L_{t_1}, L_{t_2}	1.12	mH	Input inductances
f_{sw}	4	kHz	Switching frequency

Table 3. SSOSM control parameters

Parameter	Value
m_{1_i}	0.01
m_{2_i}	0.1
m_{3_i}	1
$H_{\max_i}$	4
α_i^*	0.05

for these nodes is set equal to 380 V, while the input voltages V_{DC_1} and V_{DC_2} are both equal to 278 V. According to the stability results in Section 5, the SSOSM control parameters for the battery converters are reported in Table 3. In order to investigate the performance of the proposed control approach within a low voltage DC microgrid, four different scenarios are implemented. Note that in the following figures it is arbitrarily assumed that the current entering any node is positive (passive sign convention).

Scenario 1. Disturbance with a limited ramp rate power variation: In the first scenario it is assumed that the system is in a steady state condition with zero power absorbed by the load or provided by the generator. Each battery converter regulates its output voltage at the desired value equal to 380 V and there is no exchange of power between these two components. At the time instant $t = 5$ s the power reference for the load converter (see Fig. 5) or for the generator converter (see Fig. 6) is set to 20 kW and at the time instant $t = 35$ s, is reset to 0 kW with the ramp rate limited to 1 kW/s. As shown in the pictures, when the disturbance has a limited ramp rate, the proposed control strategy is able to keep the output voltage of both the batteries DC-DC converter to their reference without any voltage variation. When the system reaches the steady state condition, the two battery converters exchange power with the DC network in order to maintain the voltages equal to the desired values. In this situation there is not an optimal current sharing between the two battery converters because the load and the generator are not connected to the same node of the grid and different line impedances connect the components.

Scenario 2. Disturbance with a step power variation: In

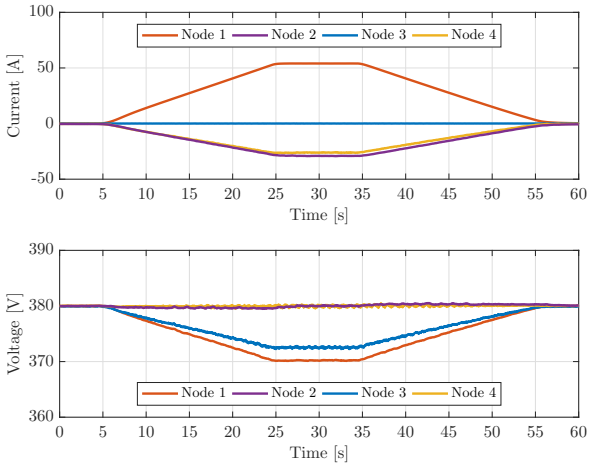

Figure 5. Scenario 1: system performance with a load variation of about 20 kW in case of ramp rate equal to 1 kW/s.

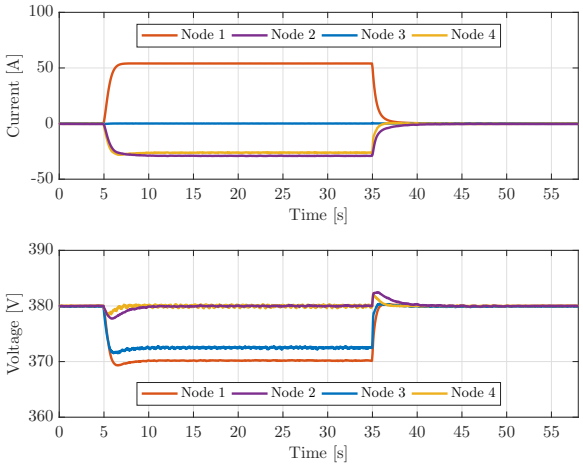

Figure 7. Scenario 2: system performance with a step load variation of about 20 kW.

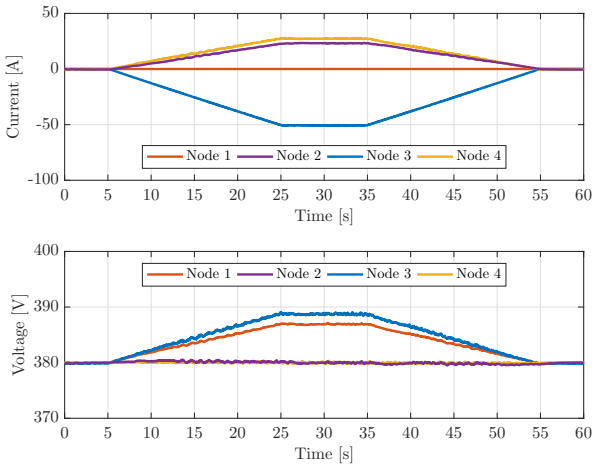

Figure 6. Scenario 1: system performance with a generator variation of about 20 kW in case of ramp rate equal to 1 kW/s.

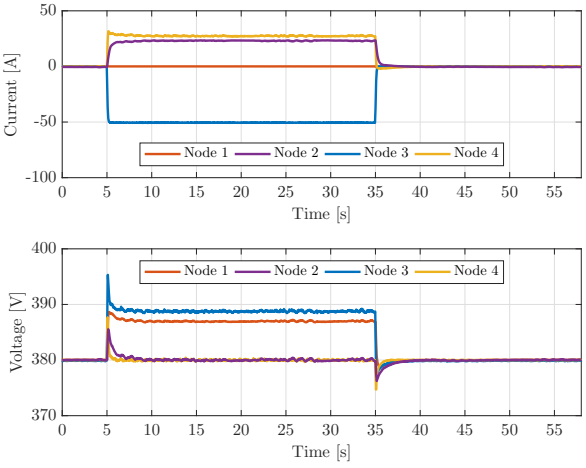

Figure 8. Scenario 2: system performance with a step generator variation of about 20 kW.

the second scenario the same tests explained in Scenario 1 are replicated without the ramp rate limitation. In this situation it is possible to see, as shown in Fig. 7 and in Fig. 8, a transient in the DC network voltages due to the step power variation of the load and the generator, respectively. The transient is different in these two cases because the dynamics of the load and the generator are different. In any case the system exhibits a stable performance thanks to the robustness of the proposed decentralized SSOSM control approach.

Scenario 3. Step variation of the voltage reference: In this third scenario it is assumed that the system is in a steady state condition with a constant power equal to 20 kW absorbed by the load or provided by the generator. Each battery converter regulates its output voltage at a fixed value equal to 380 V, and the power exchanged by the two batteries is different due to the different line impedances. At the time instant $t = 5$ s the DC voltage reference for one of the two battery converters is modified. Fig. 9 shows the system performances when the constant load is set to 20 kW and the reference voltage of the first battery converter is increased by 5 V, while Fig. 10 shows the opposite situation with the constant generation set to 20 kW and the reference voltage of the second battery converter decreased by 5 V. In these situations it is possible to observe that the DC voltage variation in one battery converter has no significant effect on the voltage at the other battery converter. The system exhibits a stable performance thanks to the robustness of the proposed decentralized SSOSM control approach. By modifying the voltage reference of the two battery converters it is possible to obtain a different current sharing among the batteries of the microgrid. As illustrated in the next scenario, it is indeed possible to cover the control objective related to optimal current sharing.

Scenario 4. Current sharing: In this scenario the proposed voltage controllers have been coupled with a higher-level con-

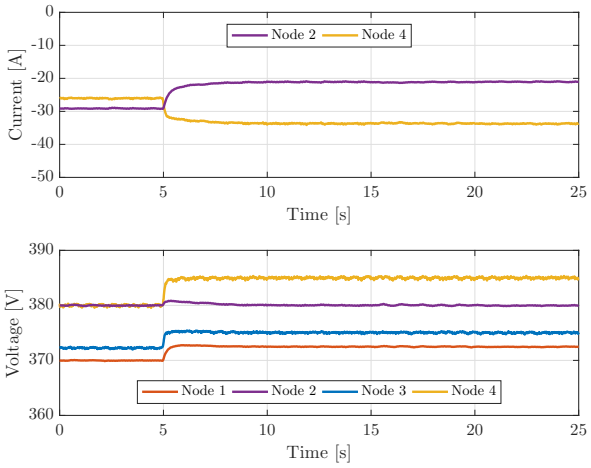

Figure 9. Scenario 3: system performance with a step DC voltage reference variation of battery converter number 1.

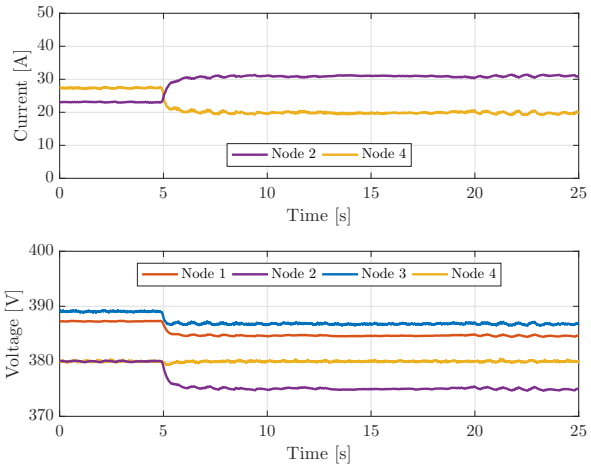

Figure 10. Scenario 3: system performance with a step DC voltage reference variation of battery converter number 2.

trol scheme that calculates the voltage references for the battery converters in order to achieve optimal current sharing among the batteries (see Fig. 11). Although the analysis of a higher-level control scheme is outside the scope of this work, Scenario 4 is aimed at showing experimentally that the proposed voltage controllers, due to their robustness property in tracking the voltage references, can be coupled with a higher-level control scheme that guarantees optimal current or power sharing.

Finally, note that in the discussed scenarios, only the voltage at Node 2 and Node 4 have been controlled with the proposed strategy. Nevertheless, the voltage deviations from the nominal value in the other two nodes (i.e. Node 1 and Node 3), depending on the line impedances, are always less than the 5% of the desired voltage value.

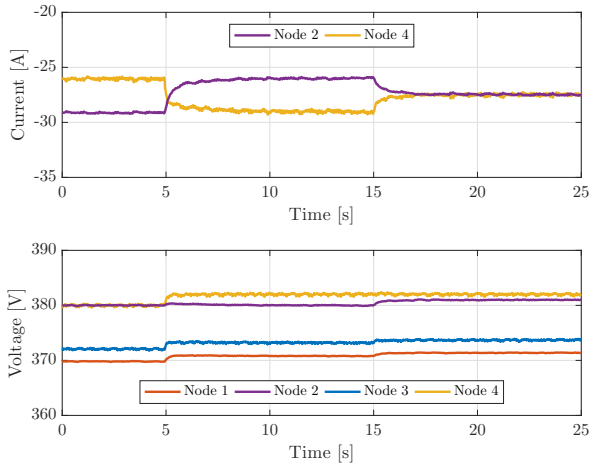

Figure 11. Scenario 4: system performance in case of constant load (20 kW) and voltage reference variation for the DC-DC battery converters in order to obtain optimal current sharing.

7. Conclusions

In this paper a robust control strategy has been designed to regulate the voltage in boost-based DC microgrids. The proposed control scheme is fully decentralized and is based on higher order sliding mode control methodology, which allows to obtain continuous control inputs. The latter can be used as duty cycles of the boost converters, achieving constant switching frequency and facilitating a PWM-based implementation. The stability of a boost-based microgrid has been theoretically analyzed proving that, on the proposed sliding manifold, the desired operating point is locally exponentially stable. The proposed control scheme has been validated through experimental tests on a real DC microgrid, showing satisfactory closed-loop performances. Interesting future research includes the stability analysis of the obtained nonlinear equivalent system, as well as studying the performance of the proposed control scheme in more heterogeneous networks, possibly including different converter types and the presence of local control strategies that differ from the one proposed here.

References

[1] T. Ackermann, G. Andersson, L. Söder, Distributed generation: a definition, Electric Power Systems Research 57 (3) (2001) 195–204.
[2] G. Pepermans, J. Driesen, D. Haeseldonckx, R. Belmans, W. D'haeseleer, Distributed generation: definition, benefits and issues, Energy Policy 33 (6) (2005) 787–798.
[3] J. P. Lopes, N. Hatziargyriou, J. Mutale, P. Djapic, N. Jenkins, Integrating distributed generation into electric power systems: A review of drivers, challenges and opportunities, Electric Power Systems Research 77 (9) (2007) 1189–1203, distributed Generation.
[4] J. M. Guerrero, F. Blaabjerg, T. Zhelev, K. Hemmes, E. Monmasson, S. Jemei, M. P. Comech, R. Granadino, J. I. Frau, Distributed generation: Toward a new energy paradigm, IEEE Industrial Electronics Magazine 4 (1) (2010) 52–64.
[5] N. L. Panwar, S. C. Kaushik, S. Kothari, Role of renewable energy sources in environmental protection: A review, Renewable and Sustainable Energy Reviews 15 (3) (2011) 1513–1524.

[6] C. Wang, S. Wang, Study on some key problems related to distributed generation systems, Automation of Electric Power Systems 20 (32) (2008) 1–4.
[7] J. M. Carrasco, L. G. Franquelo, J. T. Bialasiewicz, E. Galvan, R. C. PortilloGuisado, M. A. M. Prats, J. I. Leon, N. Moreno-Alfonso, Power-electronic systems for the grid integration of renewable energy sources: A survey, IEEE Transactions on Industrial Electronics 53 (4) (2006) 1002–1016.
[8] M. Liserre, T. Sauter, J. Y. Hung, Future energy systems: Integrating renewable energy sources into the smart power grid through industrial electronics, IEEE Industrial Electronics Magazine 4 (1) (2010) 18–37.
[9] A. Kanase-Patil, R. Saini, M. Sharma, Integrated renewable energy systems for off grid rural electrification of remote area, Renewable Energy 35 (6) (2010) 1342–1349.
[10] R. Lasseter, Microgrids, in: IEEE Power Engineering Society Winter Meeting, Vol. 1, 2002, pp. 305–308.
[11] N. Hatziargyriou, H. Asano, R. Iravani, C. Marnay, Microgrids, IEEE Power and Energy Magazine 5 (4) (2007) 78–94.
[12] F. Katiraei, M. Iravani, P. Lehn, Micro-grid autonomous operation during and subsequent to islanding process, IEEE Trans. Power Del. 20 (1) (2005) 248–257.
[13] R. Lasseter, P. Paigi, Microgrid: a conceptual solution, in: Proc. 35th IEEE Power Electron. Specialists Conf., Vol. 6, Aachen, Germany, 2004, pp. 4285–4290.
[14] M. S. Sadabadi, Q. Shafiee, A. Karimi, Plug-and-play voltage stabilization in inverter-interfaced microgrids via a robust control strategy, IEEE Transactions on Control Systems Technology 25 (3) (2017) 781–791.
[15] S. Trip, M. Bürger, C. De Persis, An internal model approach to frequency regulation in inverter-based microgrids with time-varying voltages, in: Proc. of the 53rd IEEE Conference on Decision and Control, 2014, pp. 223–228.
[16] M. Cucuzzella, G. P. Incremona, A. Ferrara, Design of robust higher order sliding mode control for microgrids, IEEE J. Emerg. Sel. Topics Circuits Syst. 5 (3) (2015) 393–401.
[17] M. Cucuzzella, G. P. Incremona, A. Ferrara, Decentralized sliding mode control of islanded ac microgrids with arbitrary topology, IEEE Transactions on Industrial Electronics 64 (8) (2017) 6706–6713.
[18] C. De Persis, N. Monshizadeh, Bregman storage functions for microgrid control, IEEE Transactions on Automatic Control 63 (1) (2018) 53–68.
[19] J. W. Simpson-Porco, F. Dörfler, F. Bullo, Synchronization and power sharing for droop-controlled inverters in islanded microgrids, Automatica 49 (9) (2013) 2603–2611.
[20] J. Schiffer, R. Ortega, A. Astolfi, J. Raisch, T. Sezi, Conditions for stability of droop-controlled inverter-based microgrids, Automatica 50 (10) (2014) 2457–2469.
[21] J. J. Justo, F. Mwasilu, J. Lee, J.-W. Jung, AC-microgrids versus DC-microgrids with distributed energy resources: A review, Renewable Sustain. Energy Rev. 24 (2013) 387–405.
[22] T. Dragicevic, J. C. Vasquez, J. M. Guerrero, D. Skrlec, Advanced lvdc electrical power architectures and microgrids: A step toward a new generation of power distribution networks., IEEE Electrification Magazine 2 (1) (2014) 54–65.
[23] X. Liu, P. Wang, P. C. Loh, A hybrid AC/DC microgrid and its coordination control, IEEE Transactions on Smart Grid 2 (2) (2011) 278–286.
[24] J. M. Guerrero, P. C. Loh, T. L. Lee, M. Chandorkar, Advanced control architectures for intelligent microgrids - part ii: Power quality, energy storage, and AC/DC microgrids, IEEE Transactions on Industrial Electronics 60 (4) (2013) 1263–1270.
[25] N. Flourentzou, V. G. Agelidis, G. D. Demetriades, Vsc-based hvdc power transmission systems: An overview, IEEE Transactions on Power Electronics 24 (3) (2009) 592–602.
[26] E. Benedito, D. del Puerto-Flores, A. Dòria-Cerezo, O. van der Feltz, J. M. A. Scherpen, Strictly convex loss functions for port-hamiltonian based optimization algorithm for mtdc networks, in: Proc. of the 55th IEEE Conference on Decision and Control, 2016, pp. 7483–7488.
[27] M. Andreasson, R. Wiget, D. V. Dimarogonas, K. H. Johansson, G. Andersson, Distributed frequency control through mtdc transmission systems, IEEE Transactions on Power Systems 32 (1) (2017) 250–260.
[28] D. Zonetti, R. Ortega, J. Schiffer, A tool for stability and power sharing analysis of a generalized class of droop controllers for high-voltage direct-current transmission systems, IEEE Transactions on Control of Network Systems.
[29] M. Cucuzzella, S. Rosti, A. Cavallo, A. Ferrara, Decentralized sliding mode voltage control in DC microgrids, in: Proc. of the American Control Conference, Seattle, WA, USA, 2017, pp. 3445–3450.
[30] S. Anand, B. G. Fernandes, J. Guerrero, Distributed control to ensure proportional load sharing and improve voltage regulation in low-voltage DC microgrids, IEEE Transactions on Power Electronics 28 (4) (2013) 1900–1913.
[31] J. Zhao, F. Dörfler, Distributed control and optimization in DC microgrids, Automatica 61 (2015) 18–26.
[32] M. Cucuzzella, S. Trip, C. De Persis, A. Ferrara, A. van der Schaft, A robust consensus algorithm for current sharing and voltage regulation in dc microgrids, arXiv preprint arXiv:1708.04608.
[33] V. Nasirian, S. Moayedi, A. Davoudi, F. L. Lewis, Distributed cooperative control of DC microgrids, IEEE Transactions on Power Electronics 30 (4) (2015) 2288–2303.
[34] M. Tucci, L. Meng, J. M. Guerrero, G. Ferrari-Trecate, A consensus-based secondary control layer for stable current sharing and voltage balancing in dc microgrids, arXiv preprintarXiv:1603.03624.
[35] M. Hamzeh, A. Ghazanfari, Y. A. R. I. Mohamed, Y. Karimi, Modeling and design of an oscillatory current-sharing control strategy in DC microgrids, IEEE Transactions on Industrial Electronics 62 (11) (2015) 6647–6657.
[36] C. De Persis, E. Weitenberg, F. Dörfler, A power consensus algorithm for DC microgrids, arXiv preprintarXiv:1611.04192.
[37] R. Han, M. Tucci, R. Soloperto, A. Martinelli, G. Ferrari-Trecate, J. M. Guerrero, Hierarchical plug-and-play voltage/current controller of dc microgrid with grid-forming/feeding converters: Line-independent primary stabilization and leader-based distributed secondary regulation, arXiv preprint arXiv:1707.07259.
[38] J. M. Guerrero, J. C. Vasquez, J. Matas, L. G. de Vicuna, M. Castilla, Hierarchical control of droop-controlled ac and dc microgrids–a general approach toward standardization, IEEE Transactions on Industrial Electronics 58 (1) (2011) 158–172.
[39] A. Mohamed, Hierarchical control for dc microgrids, in: L. Mihet-Popa (Ed.), Energy Management of Distributed Generation Systems, InTech, 2016, Ch. 03, pp. 59–77.
[40] D. O'Keeffe, S. Riverso, L. Albiol-Tendillo, G. Lightbodyt, Distributed hierarchical droop control of boost converters in dc microgrids, in: 2017 28th Irish Signals and Systems Conference, 2017, pp. 1–6.
[41] A. K. Yadav, A. Ray, M. M. Lokhande, Low-voltage dc microgrid network: A case study for standalone system, International Journal of Renewable Energy Research 7 (3) (2017) 1186–1194.
[42] V. Utkin, Sliding Modes in Control and Optimization, Communication and control engineering, Springer-Verlag, 1992.
[43] C. Edwards, S. K. Spurgen, Sliding Mode Control: Theory and Applications, Taylor and Francis, London, UK, 1998.
[44] V. Utkin, J. Guldner, J. Shi, Sliding mode control in electro-mechanical systems, Vol. 34, CRC press, 2009.
[45] H. Sira-Ramirez, M. Rios-Bolivar, Sliding mode control of dc-to-dc power converters via extended linearization, IEEE Transactions on Circuits and Systems I: Fundamental Theory and Applications 41 (10) (1994) 652–661.
[46] H. Sira-Ramírez, R. Silva-Ortigoza, Control design techniques in power electronics devices, Springer Science & Business Media, 2006.
[47] Y. B. Shtessel, A. S. I. Zinober, I. A. Shkolnikov, Boost and buck-boost power converters control via sliding modes using method of stable system centre, in: Proc. of the 41st IEEE Conference on Decision and Control, Las Vegas, NV, USA, 2002, pp. 340–345.
[48] Y. B. Shtessel, A. S. I. Zinober, I. A. Shkolnikov, Boost and buck-boost power converters control via sliding modes using dynamic sliding manifold, in: Proc. of the 41st IEEE Conference on Decision and Control, Las Vegas, NV, USA, 2002, pp. 2456–2461.
[49] A. Cavallo, B. Guida, Sliding mode control for dc/dc converters, in: Proceedings of the 51st IEEE Conference on Decision and Control, 2012, pp. 7088–7094.
[50] S.-C. Tan, Y. M. Lai, C. K. Tse, A unified approach to the design of pwm-based sliding-mode voltage controllers for basic dc-dc converters in continuous conduction mode, IEEE Transactions on Circuits and Systems I: Regular Papers 53 (8) (2006) 1816–1827.
[51] S. C. Tan, Y. M. Lai, C. K. Tse, General design issues of sliding-mode

controllers in dc–dc converters, IEEE Transactions on Industrial Electronics 55 (3) (2008) 1160–1174.
[52] B. J. Cardoso, A. F. Moreira, B. R. Menezes, P. C. Cortizo, Analysis of switching frequency reduction methods applied to sliding mode controlled dc-dc converters, in: Applied Power Electronics Conference and Exposition, 1992, pp. 403–410.
[53] A. Bartoszewicz, Discrete-time quasi-sliding-mode control strategies, IEEE Transactions on Industrial Electronics 45 (4) (1998) 633–637.
[54] J. Mahdavi, A. Emadi, H. A. Toliyat, Application of state space averaging method to sliding mode control of pwm dc/dc converters, in: Industry Applications Conference, 1997, pp. 820–827.
[55] H. E. Fadil, F. Giri, H. Ouadi, Adaptive sliding mode control of pwm boost dc-dc converters, in: IEEE Conference on Computer Aided Control System Design, IEEE International Conference on Control Applications, IEEE International Symposium on Intelligent Control, 2006, pp. 3151–3156.
[56] S. Oucheriah, L. Guo, Pwm-based adaptive sliding-mode control for boost dc–dc converters, IEEE Transactions on Industrial Electronics 60 (8) (2013) 3291–3294.
[57] R. J. Wai, L. C. Shih, Design of voltage tracking control for dc-dc boost converter via total sliding-mode technique, IEEE Transactions on Industrial Electronics 58 (6) (2011) 2502–2511.
[58] D. Ronchegalli, R. Lazzari, Development of the control strategy for a direct current microgrid: A case study, in: AEIT International Annual Conference, 2016, pp. 1–6.
[59] V. Venkatasubramanian, H. Schattler, J. Zaborszky, Fast time-varying phasor analysis in the balanced three-phase large electric power system, IEEE Transactions on Automatic Control 40 (11) (1995) 1975–1982.
[60] H. Akagi, E. H. Watanabe, M. Aredes, Instantaneous power theory and applications to power conditioning, Vol. 31, John Wiley & Sons, 2007.
[61] F. Dörfler, F. Bullo, Kron reduction of graphs with applications to electrical networks, IEEE Transactions on Circuits and Systems I: Regular Papers 60 (1) (2013) 150–163.
[62] L. Iannelli, F. Vasca, Dithering for sliding mode control of dc/dc converters, in: 2004 IEEE 35th Annual Power Electronics Specialists Conference (IEEE Cat. No.04CH37551), Vol. 2, 2004, pp. 1616–1620 Vol.2.
[63] M. Fadel, A. M. Llor, Fixed frequency sliding mode control for boost converter, in: 2006 12th International Power Electronics and Motion Control Conference, 2006, pp. 957–960.
[64] L. Wang, F. Meng, Z. Sun, S. Yang, W. Yang, An adaptive hysteresis sliding mode control method for double-switch buck-boost converter, in: IEEE Transportation Electrification Conference and Expo, 2017, pp. 1–6.
[65] G. Bartolini, A. Ferrara, E. Usai, Chattering avoidance by second-order sliding mode control, IEEE Transactions on Automatic Control 43 (2) (1998) 241–246.
[66] G. P. Incremona, M. Cucuzzella, A. Ferrara, Adaptive suboptimal second-order sliding mode control for microgrids, Int. J. Control 89 (9) (2016) 1849–1867.
[67] G. Bartolini, A. Ferrara, E. Usai, On boundary layer dimension reduction in sliding mode control of SISO uncertain nonlinear systems, in: Proc. IEEE Int. Conf. Control Applications, Trieste, Italy, 1998, pp. 242–247.
[68] A. Levant, Sliding order and sliding accuracy in sliding mode control, International Journal of Control 58 (6) (1993) 1247–1263.